



## Analysis of streaming effects in stirling-type inertance pulse tube cryocoolers using computational fluid dynamics

Rajendra Kumar, Jan G. Korvink & Jürgen J. Brandner

**To cite this article:** Rajendra Kumar, Jan G. Korvink & Jürgen J. Brandner (2025) Analysis of streaming effects in stirling-type inertance pulse tube cryocoolers using computational fluid dynamics, Engineering Applications of Computational Fluid Mechanics, 19:1, 2565796, DOI: [10.1080/19942060.2025.2565796](https://doi.org/10.1080/19942060.2025.2565796)

**To link to this article:** <https://doi.org/10.1080/19942060.2025.2565796>



© 2025 The Author(s). Published by Informa UK Limited, trading as Taylor & Francis Group.



Published online: 07 Oct 2025.



[Submit your article to this journal](#)



Article views: 132



[View related articles](#)



[View Crossmark data](#)

# Analysis of streaming effects in stirling-type inertance pulse tube cryocoolers using computational fluid dynamics

Rajendra Kumar, Jan G. Korvink and Jürgen J. Brandner

Institute of Microstructure Technology, Karlsruhe Institute of Technology, Karlsruhe, Germany

## ABSTRACT

To look inside a pulse tube for streaming effects beyond 5–6 Hz is not possible experimentally. Therefore, CFD is a reliable tool for observing the streaming effects occurring in a cryocooler. In the present work, a numerical investigation on the inertance type pulse tube cryocooler (IPTCC) is carried out using computational fluid dynamics (CFD) at frequencies greater than 80 Hz. A numerical model is developed, and simulations are validated against the numerical results published in the open literature. As opposed to the local thermal non-equilibrium model, porous media are modelled using a local thermal equilibrium approach. The streaming effects are analysed in the pulse tube for various sizes and frequencies with temperature-dependent material properties. It was observed that Rayleigh streaming is most likely to occur when the viscous penetration depth is very small compared to the pulse tube radius. Further, it was also examined that streaming is purely acoustical, not due to the transition to turbulent flow in the pulse tube. While varying the whole length of IPTCC, Rayleigh streaming occurred at a particular combination of size and frequency. Furthermore, the streaming at different time periods was analysed for two cases of different IPTCC lengths. It was found that a combination of various factors and flow conditions resulted in the appearance and disappearance of vortices in the pulse tube in various instances. The present study also suggests an interplay between the acoustic power density, size, and frequency of the IPTCC. It is concluded that CFD modelling is necessary to observe the multidimensional effects and complex transport phenomena in IPTCC.

## ARTICLE HISTORY

Received 31 December 2024  
Accepted 8 September 2025

## KEYWORDS

Cryocooler; streaming effects; CFD; local thermal equilibrium; pulse tube

## 1. Introduction

Cryocoolers are devices capable of producing temperatures below 120 K (Walker, 2014). According to the heat exchangers used in cryocoolers, they are categorised as recuperative and regenerative (Walker, 2014). Pulse tube cryocoolers (PTCC) have rapidly developed among regenerative cryocoolers. Over other regenerative cryocoolers (Stirling and Gifford-McMahon), PTCC provides the following advantages (Chakravarthy et al., 2011; Panda et al., 2023; Radebaugh, 2009):



- (1) No moving part at the cold-finger.
- (2) Higher time between the maintenance.
- (3) Absence of low-temperature seals.
- (4) Less wear and tear.

Gifford and Longworth discovered the basic PTCC in the early 1960s (Gifford & Longworth, 1964). After the advent of basic PTCC, various phase-shifting mechanisms resulted in further development of PTCC, such as orifice PTCC (Mikulin et al., 1984), inertance PTCC

(Kanao et al., 1994), double inlet PTCC (Shaowei et al., 1990), and multi-stage units (Matsubara & Gao, 1994). Various configurations of PTCC are also presented in the open literature, i.e. U-type PTCC, inline PTCC, and co-axial PTCC. The merits and demerits of each type are explained by Radebaugh (Radebaugh, 2000). The inline PTCC is the most efficient among all configurations (Radebaugh, 2000). PTCC are used in many industrial applications, such as cooling of infrared sensors for night-vision cameras, cooling of superconductors in MRI systems or high-temperature superconducting cables, production and storage of liquid cryogen for space missions, and so forth (Radebaugh, 2009).

### 1.1. Role of computational fluid dynamics in the analysis of PTCC

There are many tools available to predict the performance of PTCC. The analytical models for PTCC comprise phasor (Almtireen et al., 2020), nodal, and cyclic analyses (Choudhari et al., 2021). Higher-order numerical

**CONTACT** Rajendra Kumar  rajendra.kumar@kit.edu  Institute of Microstructure Technology, Karlsruhe Institute of Technology, Hermann-von-Helmholtz-Platz 1, Karlsruhe 76344, Germany

models comprising finite volume method discretization are more favourable for modelling and simulation of PTCC to capture 2D and 3D flow patterns arising in PTCC (Panda et al., 2023). The use of computational fluid dynamics (CFD) for the performance prediction of PTCC gained prominence after the year 2000 (Cha et al., 2006; Flake & Razani, 2004). CFD is widely used in many studies to capture the flow physics and to visualise the transport phenomena in various systems (Wang et al., 2024; L. Zhang et al., 2024; N. Zhang et al., 2024). Flake and Razani (Flake & Razani, 2004) observed recirculation patterns near the heat exchangers and streaming effects in the pulse tube using CFD. Such results cannot be obtained from one-dimensional (1D) simulations. Cha et al. used CFD for simulating the multidimensional effects occurring in IPTCC (Cha et al., 2006). They inferred that a 1D analysis is insufficient when one or more components have a relatively small length-to-diameter ratio. Ashwin et al. (2010) used the local thermal non-equilibrium model to simulate porous media of IPTCC in contrast to the local thermal equilibrium approach used by Cha et al. (2006). Ashwin et al. (2010) also observed that the finite thickness of the wall gives rise to higher temperatures at cold-end heat exchangers due to increased axial heat conduction. Chen et al. (2010) studied the thermodynamic cycles in an IPTCC using the commercial CFD package FLUENT. They used the local thermal equilibrium approach and inferred that the CFD simulations and theoretical analysis predict the same type of thermodynamic cycles at the same location; however, only CFD simulations gave quantitative results. Antao and Farouk (2011a) also used the commercial CFD package CFD-ACE+ to observe the effect of operating frequency on the performance of an orifice PTCC. They observed that non-uniform temperature profiles in the pulse tube at the optimum frequency are due to the formation of bi-cellular vortices. At higher frequencies, the bi-cellular circulation patterns were observed to increase the cooling performance of the orifice PTCC. Gu, Zhou et al. (2012) analysed the DC flow streaming occurring in the pulse tube of an IPTCC in the form of asymmetric pressure drop due to sudden enlargements and contractions. Mulcahey et al. (2012) performed 3D analysis to investigate the tilt losses associated with the orientation of PTCC using the FLUENT package. They observed that the tilt losses increased with the tilt angle, and the best configuration was achieved with the cold tip downwards. Rout et al. (2013) conducted a CFD study to investigate the effect of porosity on the performance of PTCC. Their study revealed that the best performance was achieved at a porosity of 0.6 out of the tested porosities. Fang et al. proposed a 1D-2D/3D coupling model for a coaxial PTCC (Fang et al., 2017). The components, such as

the inertance tube and buffer tank, were modelled using a 1D code, and then coupling was done with the help of FLUENT to the other components. They attributed their discrepancies to the conductive and radiative losses that were not considered. Kumar et al. compared the 2D and 3D numerical simulation of an IPTCC (P. Kumar et al., 2019). They also compared the simulation time between the piston with dynamic mesh and pressure user-defined function. It was reported in their study that using a pressure user-defined function reduces the computational time by  $\approx 25\%$ . Moreover, only a slight difference was observed between the 3D and 2D axis-symmetric simulations. Choudhari et al. investigated the phase difference between the pressure and the mass flow rate at the cold end heat exchanger exit (Choudhari et al., 2021). It was inferred that pressure and mass flow should be out of phase at the cold end of the pulse tube to attain optimum cooling performance. Zhao presented CFD results of a reservoir-less micro coaxial Stirling-type PTCC operated at 125 Hz (Zhao, 2022). It was reported that two inertial tubes could work as a phase modulator instead of a buffer tank with minor performance deterioration. Manoj et al. compared the CFD and experimental results of a GM-type double-inlet PTCC (Manoj et al., 2022). They observed that the higher average pressure resulted in lower cold-end temperatures and shorter cool-down periods. They also reported that in phase relationship between the mass flow and pressure is favoured for better machine performance.

### 1.2. Streaming effects in PTCC

Streaming effects in an IPTCC are one of the important parameters that dictate its performance. Streaming refers to a steady mass-flux density or velocity, usually of second order, that is superimposed on the larger first-order oscillating acoustic mass-flux density or velocity and is driven by the first-order oscillations (Nyborg, 1965; Swift, 2017). Primarily, there are four types of streaming in cryocoolers, namely Gedeon, Rayleigh, jet-driven streaming, and streaming within a regenerator or stack. For more details on the basics of streaming effects, readers are redirected to references (Gu, Tang et al., 2013; Swift, 2017). Researchers have tried to visualise the streaming effects in PTCC experimentally. Shiraishi, Nakamura et al. (1998) performed flow visualisation experiments with three different configurations of PTCC, i.e. BPTCC, OPTCC, and DIPTCC, at 5 Hz. Further, in another study, Shiraishi, Murakami et al. (2007) used smoke-wire for flow visualisation in an inclined DIPTCC at 6 Hz. The disadvantage of such an experimental technique is that the smoke in the pulse tube distorts at higher frequencies than 5–6 Hz. The streaming effects in



**Figure 1.** Axisymmetric computational domain, (1) Transfer line; (2) Aftercooler; (3) Regenerator; (4) Cold heat exchanger; (5) Pulse tube; (6) Hot heat exchanger; (7) Inertance tube; (8) Reservoir.

Stirling-type IPTCC have been addressed for frequencies up to 60 Hz (Gu, Zhou et al., 2012) numerically. Moudghalya et al. performed CFD simulations to show non-linear streaming effects in a coaxial type of PTCC (Moudghalya et al., 2024). The effects of the taper angle of the pulse tube were demonstrated to overcome the non-linear streaming in Stirling-type PTCC at 34 Hz (Antao & Farouk, 2011b) and 80 Hz (Yan et al., 2020). Recently, R. Kumar et al. (2024) and Moudghalya et al. (2024) have shown the importance of CFD studies to observe the streaming effects in two-stage co-axial PTCC and single-stage IPTCC, respectively. The literature review shows that CFD is a powerful and extensively used tool for analysing the multidimensional effects occurring in a PTCC.

So far, the streaming effects have not been examined at higher frequencies ( $> 80$  Hz) for Stirling-type IPTCC. In the present study, the streaming effects at frequencies greater than 50 Hz (50 Hz–200 Hz) while reducing the size of the IPTCC is undertaken.

## 2. Numerical model

The following assumptions have been employed to simplify the governing equations.

- (1) Axisymmetric fluid flow and heat transfer.
- (2) Packing is isotropic and homogeneous.
- (3) Working gas is an ideal gas.
- (4) The working gas is Newtonian.
- (5) Local thermal equilibrium exists within the porous region.

Figure 1 shows the axisymmetric computational domain used in the present study.

### 2.1. Governing equations

The PTCC consists of porous and non-porous zones. The cold heat exchanger, regenerator, and hot heat exchanger are modelled as porous zones. On the other hand, the transfer line, pulse tube, inertance tube, and reservoir are modelled as non-porous regions (open channels). The following set of governing equations is used for the porous regions.

- Continuity equation:

$$\frac{\partial(\epsilon\rho)}{\partial t} + \nabla \cdot (\rho \vec{u}) = 0 \quad (1)$$

Where,  $\epsilon$  is porosity,  $\rho$  is density of the working gas,  $\vec{u}$  is the velocity vector.

- Momentum equation:

$$\begin{aligned} \frac{\partial}{\partial t}(\rho \vec{u}) + \frac{1}{\epsilon} \nabla \cdot (\rho \vec{u} \vec{u}) \\ = -\nabla \epsilon p + \nabla \cdot \bar{\bar{\tau}} - \epsilon \left( \frac{\mu}{K} \vec{u} + \frac{C_2}{2} \rho |\vec{u}| \vec{u} \right) \end{aligned} \quad (2)$$

Where,  $p$  is pressure,  $\bar{\bar{\tau}}$  is stress tensor,  $\mu$  is dynamic viscosity of the working gas, and the permeability ( $K$ ) and the inertial ( $C_2$ ) resistance factor are given by the following equations (Zhao & Dang, 2016).

$$K = \frac{d_h^2}{64} \quad (3)$$

$$C_2 = \frac{2.91}{d_h} Re^{-0.103} \quad (4)$$

Here, Where,  $d_h$  is the hydraulic diameter of the mesh screens,  $d_w$  is the wire diameter of the mesh screens, and  $Re$  is the Reynolds number.

$$d_h = \frac{\epsilon}{(1 - \epsilon)} d_w \quad (5)$$

$$Re = \frac{\rho u d_h}{\mu} \quad (6)$$

- Energy equation:

$$\frac{\partial}{\partial t}(\rho E)_{\text{eff}} + \nabla \cdot [\vec{u}(\rho_f E_f + p)] = \nabla \cdot (k_{\text{eff}} \nabla T + \bar{\bar{\tau}} \cdot \vec{u}) \quad (7)$$

where

$$(\rho E)_{\text{eff}} = \epsilon \rho_f E_f + (1 - \epsilon) \rho_s E_s \quad (8)$$

$$k_{\text{eff}} = \epsilon k_f + (1 - \epsilon) k_s \quad (9)$$

Where,  $E$  is total energy,  $k_{\text{eff}}$  is the effective thermal conductivity,  $T$  is the total temperature,  $\rho_s$  is the density of the solid.

For the open channels, the following set of governing equations are employed.

- Continuity equation:

$$\frac{\partial \rho}{\partial t} + \nabla \cdot (\rho \vec{u}) = 0 \quad (10)$$

- Momentum equation:

$$\frac{\partial}{\partial t}(\rho \vec{u}) + \nabla \cdot (\rho \vec{u} \vec{u}) = -\nabla p + \nabla \cdot \vec{\tau} \quad (11)$$

where,

$$\vec{\tau} = \mu \left[ (\nabla \vec{u} + \nabla \vec{u}^T) + \frac{2}{3} \nabla \cdot \vec{u} \vec{I} \right] \quad (12)$$

- Energy equation:

$$\frac{\partial}{\partial t}(\rho E) + \nabla \cdot [\vec{u}(\rho E + p)] = \nabla \cdot (k \nabla T + \vec{\tau} \cdot \vec{u}) \quad (13)$$

where,

$$E = h - \frac{p}{\rho} + \frac{u^2}{2} \quad (14)$$

## 2.2. Initial and boundary conditions

For the initial conditions, the temperature of PTCC was set to 300 K, and the initial charge pressure was set to 2.5 MPa. The working fluid is considered to be Helium. Perfect cooling is assumed at the aftercooler. No load condition is applied at the CHX. All the walls, except for the HHX and aftercooler, are assumed to be adiabatic. The HHX is considered to be at 300 K. Most of the studies have modelled the compressor of the PTCC with dynamic meshing; however, P. Kumar et al. (2019) showed that using a pressure-inlet user-defined function could reduce the computational time by  $\approx 25\%$ . Therefore, a pressure-inlet udf of the form  $p = p_0 + p_1 \sin(2\pi ft)$ , where  $p_0$  is the mean pressure (2.5 MPa),  $p_1$  is the pressure amplitude (0.3 MPa),  $f$  is the frequency of operation (50, 100, 150, and 200 Hz), and  $t$  is the time, was used.

## 2.3. Solution methodology

The coupled set of governing equations mentioned above are solved using the finite volume method (Patankar, 2018). Computations were performed using the FVM-based academic version of the commercial CFD package ANSYS-Fluent<sup>®</sup> 2023R1. Table 1 shows the solvers used for the discretization of the governing equations. The pressure-based solver in Fluent<sup>®</sup> was selected. Further, SIMPLE scheme was opted for pressure-velocity coupling. PREsture STaggering Option (PRESTO!) scheme was opted for pressure interpolation. The continuity and momentum equation convergence criteria were set to  $10^{-4}$ ; for the energy equation, it was set to  $10^{-6}$ .

**Table 1.** Selected solvers for model equations in ANSYS-Fluent<sup>®</sup>.

Parameters	Solvers/Options
Momentum equation: Porous media	Superficial velocity formulation
Solver	Pressure-based
Pressure-velocity Coupling	SIMPLE
Gradient	Least squares cell based
Pressure interpolation	PRESTO!
Spatial terms in momentum and energy equation	Second order upwind discretization
Temporal	Second order implicit

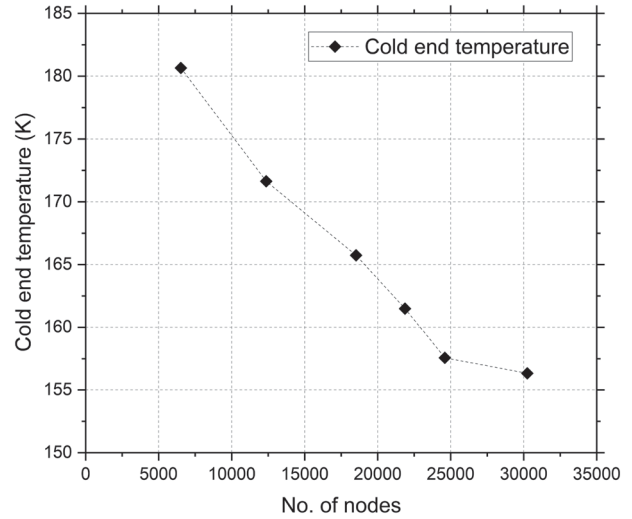


**Figure 2.** Cold end temperature at various number of nodes.

## 3. Results and discussions

The simulation results are presented in this section. The first subsection shows the grid independence study, followed by model validation and parametric studies in the later subsections.

### 3.1. Grid independence study

A grid independence study was carried out to ensure the accuracy of the numerical simulations for all the simulation runs. The cold end temperature was compared for the number of nodes 6526, 12370, 18520, 21870, 24605, and 30245. Figure 2 shows the cold end temperature at the different number of nodes after 18 s. The grids were refined until the temperature difference results from two successive grids came within  $\pm 1.3$  K. The imposed limit signifies the permissible tolerance limit of an industrial standard PT100 RTD according to IEC-751 class-B up to 73 K (IEC, 1986). Therefore, the mesh model with 24605 nodes for model validation was selected. The grid independence studies were performed based on the values given by Ashwin et al. (2010) (Tables 2 and 3).



**Table 2.** Geometry details and boundary conditions (Ashwin et al., 2010; Cha et al., 2006).

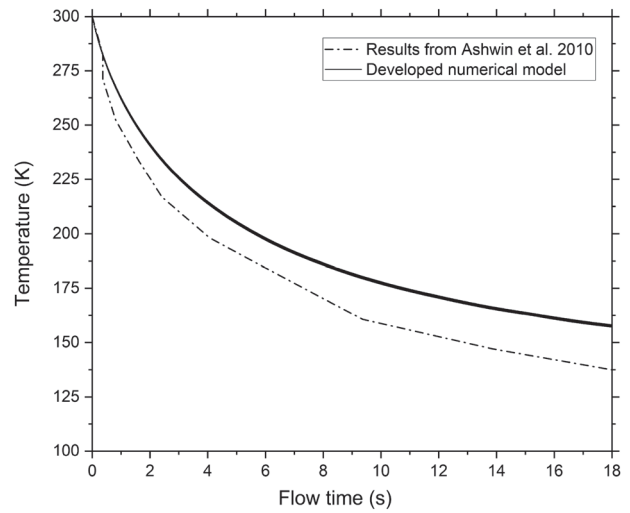
Components	Diameter (mm)	Length (mm)	Boundary condition
Transfer line (1)	2	100	Adiabatic
Aftercooler (2)	6	16	300 K
Regenerator (3)	6	60	Adiabatic
Cold heat exchanger (4)	4	4	Adiabatic
Pulse tube (5)	4	30	Adiabatic
Hot heat exchanger (6)	4	15	300 K
Inertance tube (7)	0.6	300	Adiabatic
Buffer (8)	30	80	Adiabatic

**Table 3.** Porous zones characteristics.

Component	Material	Porosity	Heat transfer model
Aftercooler	Copper	0.67	Thermal equilibrium
Regenerator	SS-304	0.65	Thermal equilibrium
Cold heat exchanger	Copper	0.67	Thermal equilibrium
Hot heat exchanger	Copper	0.67	Thermal equilibrium

### 3.2. Model validation

The numerical model is validated against the numerical data from Ashwin et al. (2010). The simulation parameters, geometry, and boundary conditions are mentioned in Table 2. The porous zone materials, porosity, and heat transfer model used are mentioned in Table 3. The temperature-dependent material properties are taken from the open literature. Table 4 shows the sources of thermophysical properties for the various materials used in the PTCC simulation. It should be noted that the material properties used in the present work are different from those of reference (Ashwin et al., 2010). For the model validation, a total of 24605 nodes were used. A time step size of 0.0003 was used with 20 inner iterations per time step, and the simulation was run for 18 s as it is done in reference (Antao & Farouk, 2011a). It is assumed that the simulations reach quasi-steady-state after 18 s (Antao & Farouk, 2011a). A computer having a CPU speed of 2000 MHz, 24 cores, and 128 GB of RAM was used for the simulation runs. The simulation took four days to complete. Figure 3 compares the cooldown behaviour of the developed numerical model with that of Ashwin et al.'s results (Ashwin et al., 2010). It can be seen from the Figure 3 that there is a discrepancy from the data of reference (Ashwin et al., 2010). The discrepancy may come from the use of different sources of thermophysical data used in the developed numerical model. Furthermore, Ashwin et al. (2010) used the local thermal non-equilibrium (LTNE) model, whereas the local thermal equilibrium (LTE) model is used in the present study. As a note, the selection of LTNE model results in co-existing temperature fields over a single physical domain, which poses a challenge in selecting a single temperature over

**Figure 3.** Comparison of cold end temperature evolution of developed numerical model to the results from Ashwin et al. (2010).

the domain. Common practices reported in the literature comprise reporting two temperature profiles (Antao & Farouk, 2011a, 2011b) or considering the mean temperature of working gas-packing material obtained from the model predictions. However, considerable uncertainties may arise at the expense of more computational cost in the case of LTNE models, where two energy equations are solved. Therefore, it is expected that modelling energy transport in porous media at cryogenic conditions using the LTE approach should result in satisfactory performance prediction and be less computationally intensive. Banded temperature profiles similar to Antao and Farouk (2011a) were observed in the present simulations. The temperature at the end of the simulation time is considered as the steady-state temperature from the banded temperature profile. The authors acknowledge that the present study lacks a comparison to the experimental data. However, there is no complete set of data for a single-stage inline Stirling-type pulse tube cryocooler, where geometry and porous media parameters (permeability and drag factor) are available. The authors are currently working on building an experimental setup to study the problem, but that study is beyond the scope of the current work.

### 3.3. Parametric studies

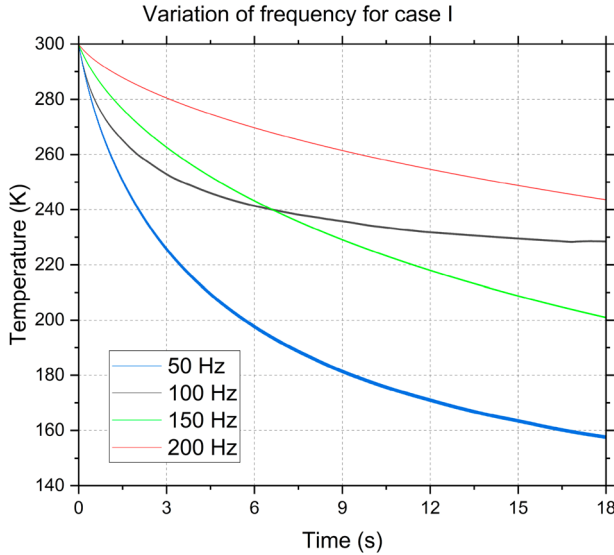
The validated numerical model was used to carry out parametric studies by varying the pulse tube cryocooler's operating frequency at various length scales of IPTCC. The operating frequency was varied between 50 Hz and 200 Hz at an interval of 50 Hz. The aspect ratio of IPTCC is defined by Equation (15) for the present study. Table 5

**Table 4.** Sources of temperature-dependent material properties.

Properties	Specific heat	Thermal conductivity	Density	Viscosity
OFHC-Cu	(Marquardt et al., 2002)	(Marquardt et al., 2002)	(Tishin & Spichkin, 2016)	–
SS-304	(Marquardt et al., 2002)	(Marquardt et al., 2002)	(Tishin & Spichkin, 2016)	–
Helium gas	(Mc Carty, 1973)	(Mc Carty, 1973)	(Mc Carty, 1973)	(Mc Carty, 1973)

**Table 5.** Parametric case studies.

Case	Length of IPTCC (mm)	PT length (mm)	PT diameter (mm)	Aspect ratio
Case I	605	30	4	7.50
Case II	302.50	15	2	7.50

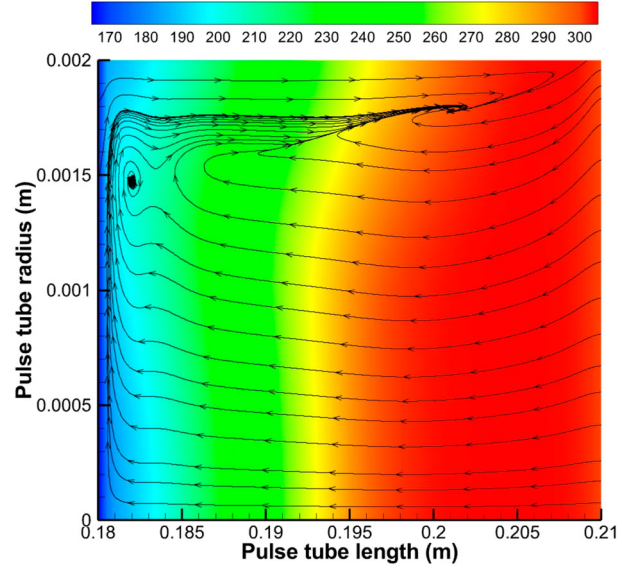
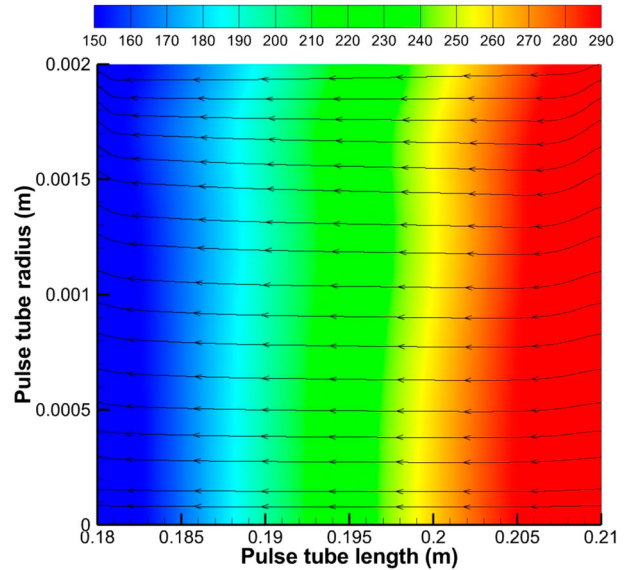
**Figure 4.** Evolution of CHX wall temperature for selected frequencies for case I.

shows the cases that are used to carry out the parametric studies. It can be seen from Table 5 that the length of the IPTCC is scaled to half while keeping the aspect ratio the same, thereby decreasing the size of the IPTCC.

$$\text{Aspect ratio} = \frac{L_c}{d_c} = \frac{\text{Length of pulse tube}}{\text{Diameter of pulse tube}} \quad (15)$$

### 3.3.1. Effect of varying operating frequency for case I

This section discusses the temperature evolution at CHX for various operating frequencies for case I. Figure 4 shows the cool-down behaviour at the operating frequencies of 50 Hz, 100 Hz, 150 Hz, and 200 Hz. It can be observed that the lowest cooling temperature ( $\approx 157$  K) is achieved at 50 Hz. The worst cooling performance is achieved at 200 Hz ( $\approx 243$  K) at the end of the simulation time. The temperature field and streamlines at the end of the simulation time within the pulse tube were looked at for each frequency at the selected aspect ratio to determine the reason behind such cooldown behaviour. Figure 5 shows the temperature contour and streamlines

**Figure 5.** Temperature contours and streamlines in the pulse tube at 50 Hz.**Figure 6.** Temperature contours and streamlines in the pulse tube at 100 Hz.

in the pulse tube at 50 Hz. It can be seen that there are two bicellular streaming structures present in the upper part of the pulse tube. This type of vortices in the pulse tube suggests that Rayleigh streaming occurs at 50 Hz. Figure 6 shows the temperature contour and streamlines

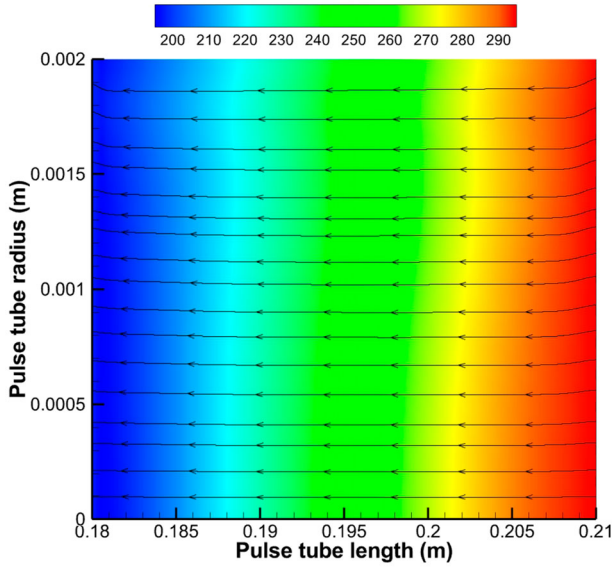


**Figure 7.** Temperature contours and streamlines in the pulse tube at 150 Hz.

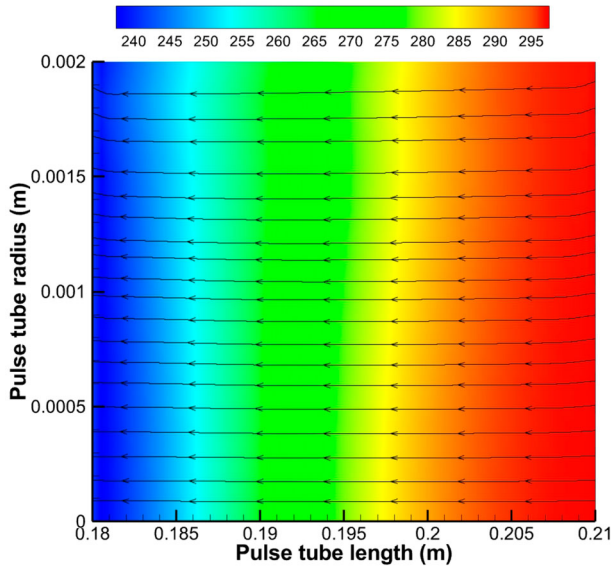


**Figure 8.** Temperature contours and streamlines in the pulse tube at 200 Hz.

in the pulse tube at 100 Hz. It can be seen that no vortices are formed in this case, unlike at 50 Hz. Figures 7 and 8 show the temperature contours and streamlines for 150 Hz and 200 Hz, respectively. It can be seen that no recirculation zones are observed at 150 Hz and 200 Hz. No vortices form at higher frequencies for case I. This may be attributed to the fact that at a particular size of IPTCC, there is an optimum frequency at which streaming occurs. The streaming effects in the pulse tube may occur if the flow becomes turbulent. However, in the present analysis, the oscillatory Reynolds number was

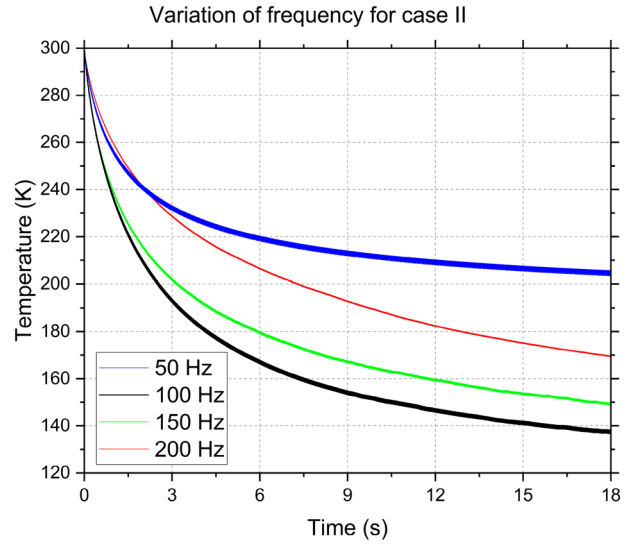


**Figure 9.** Evolution of CHX wall temperature for selected frequencies for case II.

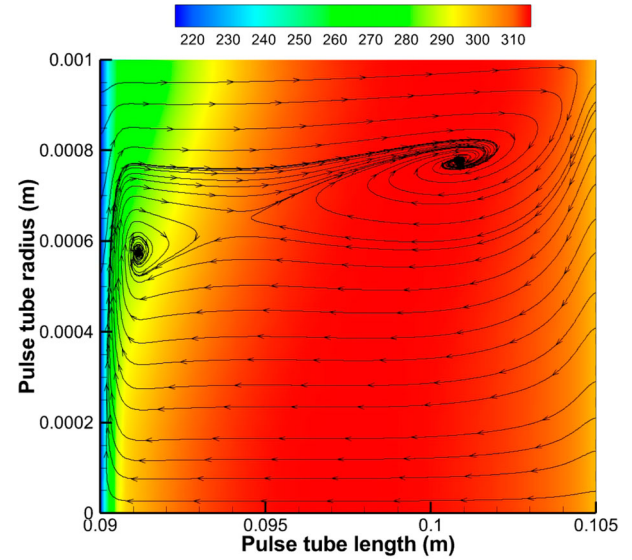


**Figure 10.** Temperature contours and streamlines in the pulse tube at 50 Hz.

calculated by Equation (16), where  $Re_o$  is the oscillatory Reynolds number,  $U_o$  is the peak velocity,  $\delta_v$  is the viscous penetration depth, and  $\nu$  is the kinematic viscosity of the working gas.

$$Re_o = \frac{U_o \delta_v}{\nu} \quad (16)$$

The maximum  $Re_o$  was 30 observed at a frequency of 50 Hz, which is well below the critical Reynolds number for oscillatory flows in a tube (Swift, 2017). Therefore, it is concluded that the streaming is purely due to the dimension and the frequency. Secondly, to examine the



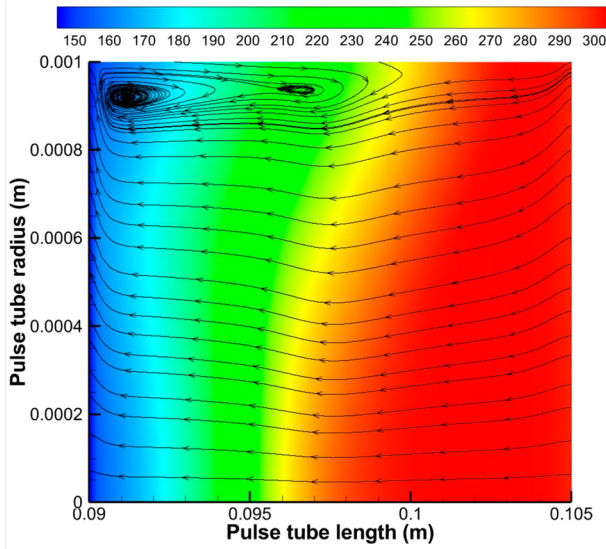


**Figure 11.** Temperature contours and streamlines in the pulse tube at 100 Hz.

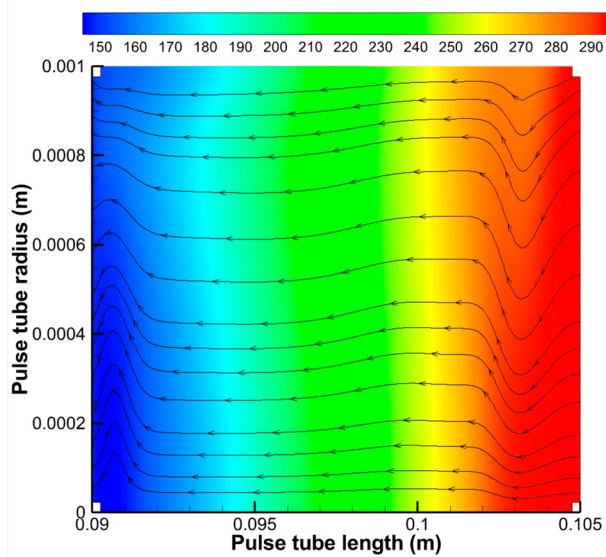


**Figure 12.** Temperature contours and streamlines in the pulse tube at 150 Hz.

existence of Rayleigh streaming in the pulse tube, the viscous penetration depth and the tube radius are compared as shown in Table 6. The viscous penetration depth is calculated by Equation (17), where  $\omega = 2\pi f$  is the angular frequency.

$$\delta_v = \sqrt{\frac{2\nu}{\omega}} \quad (17)$$

It can be observed from Table 6 that the tube-radius is greater than the viscous penetration depth by an order of magnitude. Hence, it is evident that Rayleigh streaming occurs under the conditions employed in the simulations at a particular frequency.

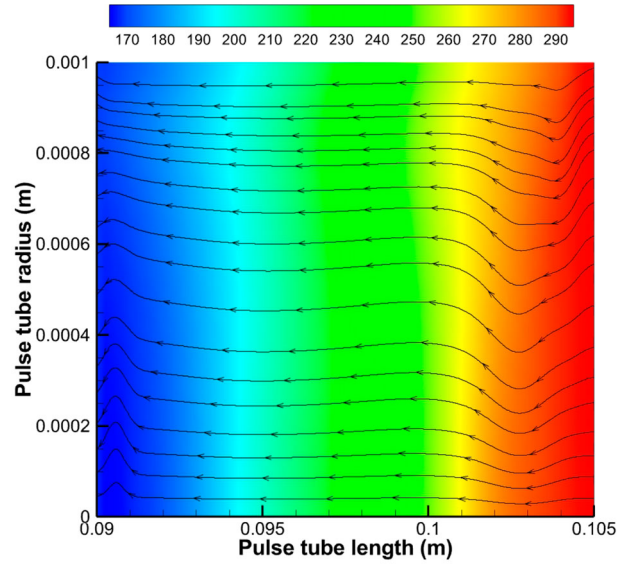


**Figure 13.** Temperature contours and streamlines in the pulse tube at 200 Hz.

**Table 6.** Viscous penetration depths for various frequencies.

Frequency Hz	Viscous penetration depth m	Tube radius m
50	0.00046	0.002
100	0.00032	0.002
150	0.00026	0.002
200	0.00023	0.002

### 3.3.2. Effect of varying operating frequency for case II

The geometry of the IPTCC was scaled to half of the original size while keeping the aspect ratio the same. The simulations were run for 50 Hz, 100 Hz, 150 Hz, and 200 Hz. Figure 9 shows the cooldown behaviour of IPTCC for case II at the selected frequencies. It can be observed that the best performance (lowest temperature at CHX) is achieved at 100 Hz ( $\approx 137$  K), whereas the worst cooling performance is observed at 50 Hz ( $\approx 205$  K). Similar to the observation in the above section, no clear trend is observed for the cooldown behaviour of the IPTCC. Figures 10 and 11 show the temperature contours and streamlines at 50 Hz and 100 Hz, respectively, for reduced aspect ratio. It is evident from Figures 10 and 11 that Rayleigh streaming is dominant in both cases with vortices. Despite the dominance of Rayleigh streaming at 50 Hz, its cooldown temperature is worse than at 100 Hz. This is because, at reduced aspect ratio and low frequency, the region of the gas plug is not sufficiently large enough to separate the cold and hot region, as seen from Figure 10. Further, high thermal transfer is not possible at 50 Hz since most of the region in the pulse tube remains undisturbed. This behaviour may be due to the excessive destruction of the boundary layer and the over-reduction of thermal stratification in the pulse tube. However, in the

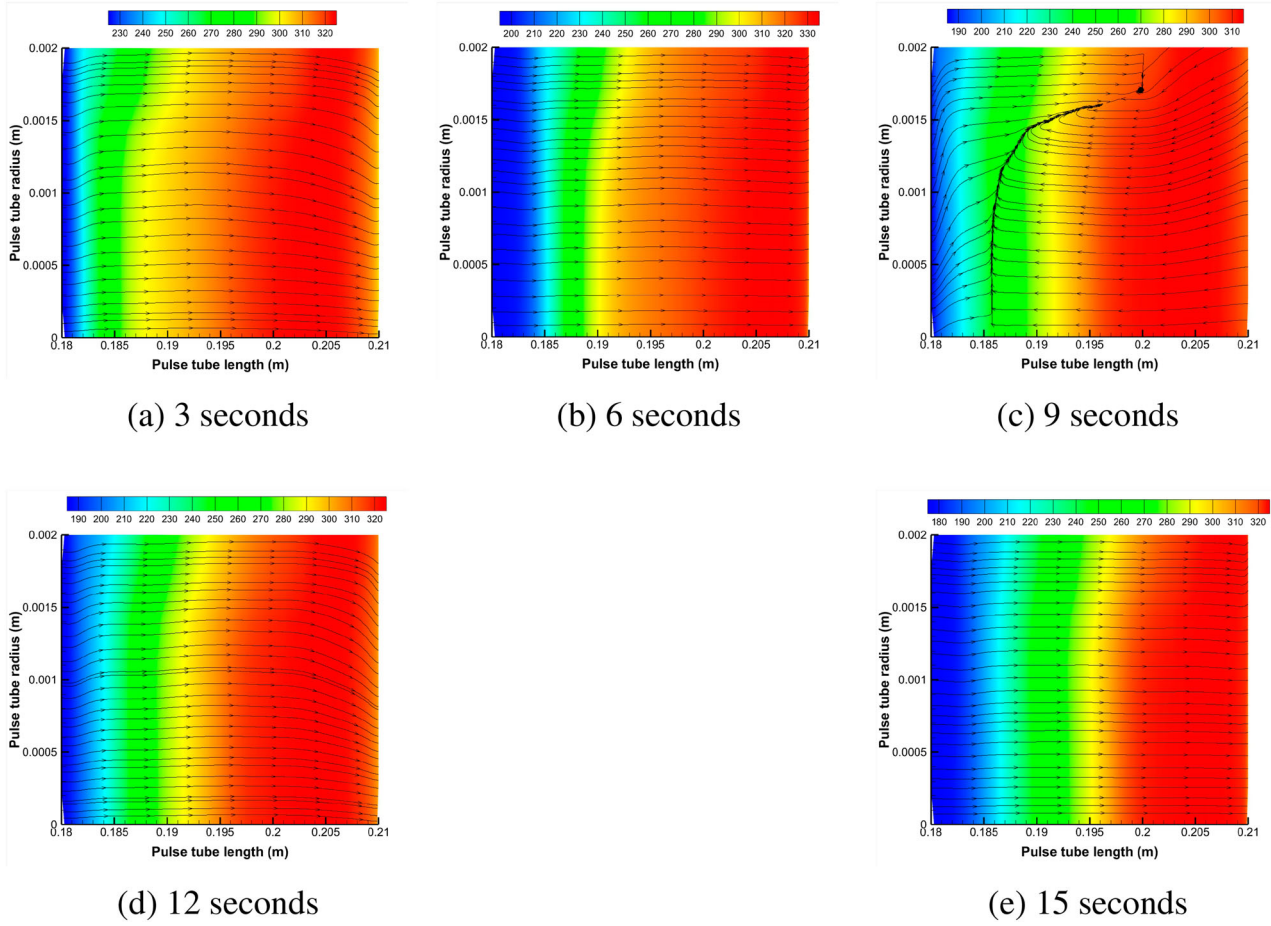


**Figure 14.** Temperature contours and streamlines for case I at 50 Hz for various time steps. (a) 3 s (b) 6 s (c) 9 s (d) 12 s (e) 15 s.

case of 100 Hz, a sufficiently large gas plug region helps separate the cold and hot regions within the pulse tube, thereby maintaining proper energy transport. Figures 12 and 13 show the temperature contours and streamlines at 50 Hz and 100 Hz, respectively. It can be observed in Figure 12 that the streamlines are curved instead of straight, hinting at the setting up of Rayleigh streaming. A similar trend is observed at 200 Hz in Figure 13. The lowest temperatures achieved at 150 Hz and 200 Hz are 148 K and 169 K. Although the performance of IPTCC is not the best at 150 Hz and 200 Hz, the simulation results indicate that when the size of IPTCC reduces with increasing frequency, better performance could be achieved.

### 3.3.3. Analysis of secondary flows in pulse tube for case I and II

To investigate the streaming effects in PTCC further, the streaming patterns at different times were plotted for case I and case II for 50 Hz and 100 Hz, respectively. Figures 14 and 15 show the temperature contours and streamlines at 3, 6, 9, 12, and 15 s for 50 Hz (case I) and 100 Hz (case II), respectively. The streamlines in both figures show some

interesting patterns. In Figure 14, it is seen that the no streaming is seen at 3 s and 6 s; however, at 9 s, there exists a recirculation zone near the wall towards the hot end of the pulse tube. Again, at 12 and 15 s, the recirculation zones disappear. The same pattern of the recirculation zone is observed in case II (100 Hz) in Figure 15. This type of behaviour suggests that the compression of the working gas occurs in the pulse tube at 9 s and gives rise to vortex formation. However, the disappearance of the vortices suggests that flow reversal may have occurred as a result of a change in flow conditions in which the vortices disappeared. Further, there are mechanisms such as pressure gradient imbalance, flow separation-reattachment, acoustic streaming, viscous dissipation and diffusion, and geometric influence, which result in the formation and disappearance of vortices in the pulse tube during a cyclic operation. Further, it is observed from Figures 14 and 15 that similar characteristics for streamlines are exhibited at different instances for case I and II. This is due to the fact that aspect ratio is kept constant for case I and II, however, length of the whole cryocooler is scaled down. Therefore, merely changing the length of the whole

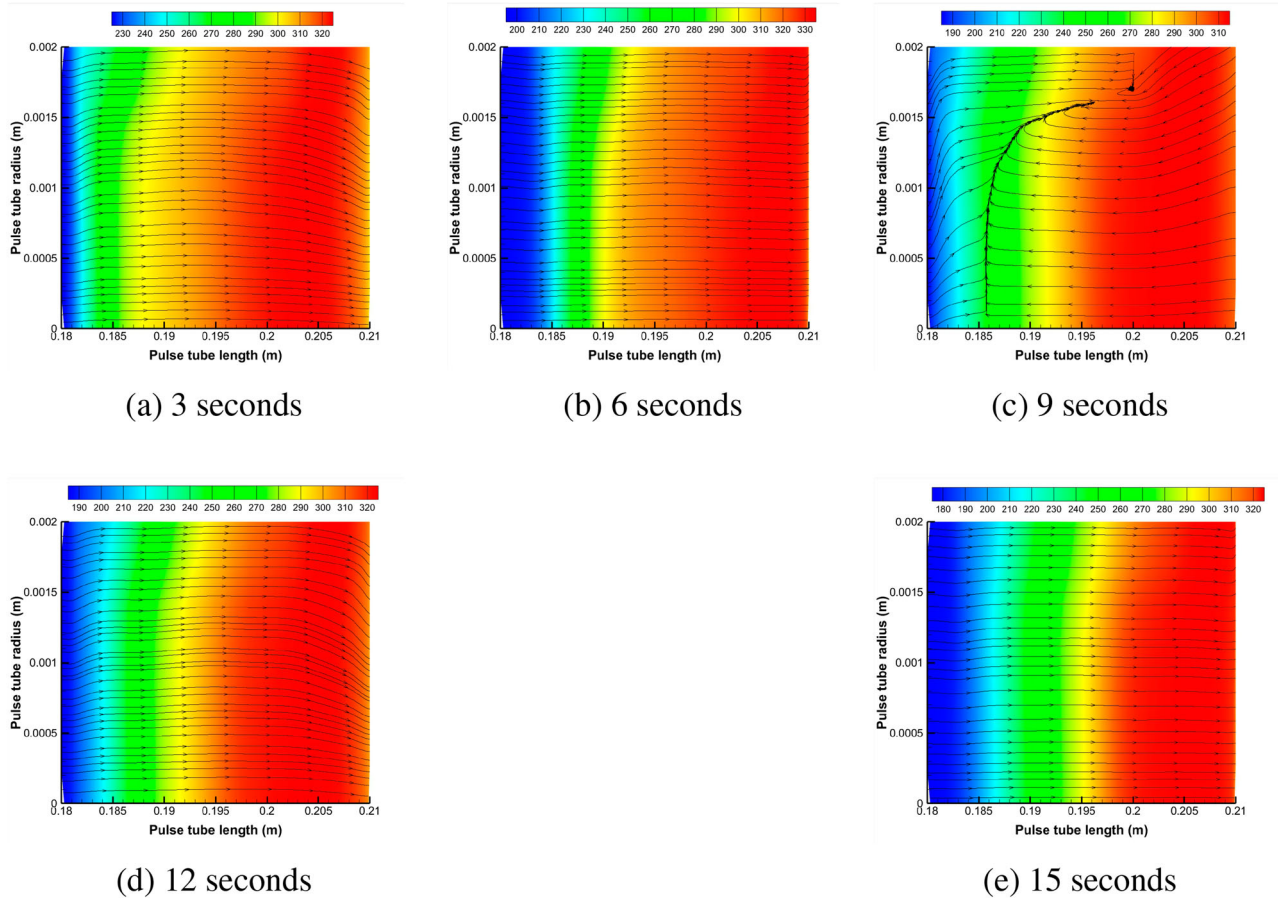


**Figure 15.** Temperature contours and streamlines for case II at 100 Hz for various time steps. (a) 3 s (b) 6 s (c) 9 s (d) 12 s (e) 15 s.

cryocooler does not bring significant changes in flow patterns unless the aspect ratio of pulse tube has not been changed.

#### 4. Conclusions, limitations, and scope of future work

A numerical model for the performance estimation of an inertance-type pulse tube cryocooler (IPTCC) was developed. The heat exchangers were modelled as porous media. A Brinkman-Forchheimer-extended Darcy equation was adopted to model the flow fields in the porous media, whereas the local thermal equilibrium approach was used to model temperature fields in the porous medium. The model was validated against the numerical results published in the open literature. The validated model was then used to observe the streaming effects by varying the length and operating frequency of the IPTCC. The streaming effects can occur during the cooldown of the cryocooler and when the cryocooler reaches a quasi-steady state. For a particular size of IPTCC, there exists a frequency at which Rayleigh streaming occurs. The condition for Rayleigh streaming is well-satisfied as per the prevailing conditions. The flow

patterns in the pulse tube change over time as a result of a combination of various factors already discussed above. Such behaviour suggests that vortex formation is very sensitive to the flow conditions and may change over time for a working cryocooler. Moreover, flow reversal and phase shift may affect the streaming patterns in the pulse tube. Rayleigh streaming occurs at a particular combination of size and frequency of the IPTCC. The cooldown curves were also plotted for various frequencies and sizes of IPTCC. The current study does not take into account the retuning of inertance tube length/diameter to achieve the optimal phase angle of the system. This has been done to isolate and analyse the effect of size and frequency only, while minimising the number of changing variables. Further, since analysis of the streaming effect is the primary focus of the present work, the energy distribution and enthalpy flow analyses are out of the scope of the present work. The simulation results showed that higher-order models, such as CFD analysis, would be necessary to capture multidimensional effects and complex transport phenomena in a Stirling type inertance pulse tube cryocooler. The present work focuses on the transient simulations of IPTCC, which are computationally intensive. In the future, the authors plan to implement the



harmonic balance method, which is computationally less intensive, to evaluate the streaming effects in pulse tube cryocoolers.

## Acknowledgments

RK acknowledges technical discussions with Dr. Georges Saliba regarding CFD simulations. All authors acknowledge support by the KIT Publication Fund of the Karlsruhe Institute of Technology, Germany.

## Data availability statement

Data will be made available upon reasonable request.

## Disclosure statement

No potential conflict of interest was reported by the author(s).

## Funding

This project is funded by the Deutsche Forschungsgemeinschaft (DFG, German Research Foundation) – SFB 1527/1 – project-ID 454252029.

## References

- Almtireen, N., Brandner, J., & Korvink, J. (2020). Pulse tube cryocooler: Phasor analysis and one-dimensional numerical simulation. *Journal of Low Temperature Physics*, 199(5-6), 1179–1197. <https://doi.org/10.1007/s10909-020-02378-6>
- Antao, D. S., & Farouk, B. (2011a). Computational fluid dynamics simulations of an orifice type pulse tube refrigerator: Effects of operating frequency. *Cryogenics*, 51(4), 192–201. <https://doi.org/10.1016/j.cryogenics.2011.02.001>
- Antao, D. S., & Farouk, B. (2011b). Numerical simulations of transport processes in a pulse tube cryocooler: Effects of taper angle. *International Journal of Heat and Mass Transfer*, 54(21-22), 4611–4620. <https://doi.org/10.1016/j.ijheatmasstransfer.2011.06.016>
- Ashwin, T., Narasimham, G., & Jacob, S. (2010). CFD analysis of high frequency miniature pulse tube refrigerators for space applications with thermal non-equilibrium model. *Applied Thermal Engineering*, 30(2-3), 152–166. <https://doi.org/10.1016/j.applthermaleng.2009.07.015>
- Cha, J., Ghiaasiaan, S., Desai, P., Harvey, J., & Kirkconnell, C. (2006). Multi-dimensional flow effects in pulse tube refrigerators. *Cryogenics*, 46(9), 658–665. <https://doi.org/10.1016/j.cryogenics.2006.03.001>
- Chakravarthy, V. S., Shah, R. K., & Venkatarathnam, G. (2011). A review of refrigeration methods in the temperature range 4–300 K. *Journal of Thermal Science and Engineering Applications*, 3(2):020801. <https://doi.org/10.1115/1.4003701>
- Chen, L., Zhang, Y., Luo, E., Li, T., & Wei, X. (2010). CFD analysis of thermodynamic cycles in a pulse tube refrigerator. *Cryogenics*, 50(11-12), 743–749. <https://doi.org/10.1016/j.cryogenics.2010.08.004>
- Choudhari, M. S., Gawali, B., & Malwe, P. (2021). Numerical analysis of inertance pulse tube refrigerator. In *IOP Conference Series: Materials Science and Engineering* (Vol. 1104, p. 012008). IOP Publishing.
- Fang, T., Spoor, P., & Ghiaasiaan, S. (2017). A computational approach for coupled 1D and 2D/3D CFD modelling of pulse Tube cryocoolers. In *IOP Conference Series: Materials Science and Engineering* (Vol. 278, p. 012172). IOP Publishing.
- Flake, B., & Razani, A. (2004). Modeling pulse tube cryocoolers with CFD. In *AIP Conference Proceedings* (Vol. 710, pp. 1493–1499). American Institute of Physics.
- Gifford, W., & Longworth, R. (1964). Pulse-tube refrigeration. *Journal of Engineering for Industry*, 86(3), 264–268. <https://doi.org/10.1115/1.3670530>
- Gu, C., Tang, J., Wang, J., & Zhou, Y. (2013). Advance in research of several types of streaming of pulse tube refrigerators. *Science China Technological Sciences*, 56(11), 2690–2701. <https://doi.org/10.1007/s11431-013-5327-x>
- Gu, C., Zhou, Y., Wang, J., Ji, W., & Zhou, Q. (2012). CFD analysis of nonlinear processes in pulse tube refrigerators: Streaming induced by vortices. *International Journal of Heat and Mass Transfer*, 55(25-26), 7410–7418. <https://doi.org/10.1016/j.ijheatmasstransfer.2012.07.085>
- IEC (1986). *Industrial platinum resistance thermometer sensors*. International Electrotechnical Commission.
- Kanao, K., Watanabe, N., & Kanazawa, Y. (1994). A miniature pulse tube refrigerator for temperatures below 100 K. *Cryogenics*, 34, 167–170. [https://doi.org/10.1016/S0011-2275\(05\)80035-9](https://doi.org/10.1016/S0011-2275(05)80035-9)
- Kumar, P., Gupta, A., Sahoo, R., & Jena, D. (2019). Numerical investigation of a 3D inertance pulse tube refrigerator from design prospective. *Cryogenics*, 98, 125–138. <https://doi.org/10.1016/j.cryogenics.2018.12.004>
- Kumar, R., Korvink, J. G., & Brandner, J. J. (2024). Computational fluid dynamic simulations of miniature pulse tube cryocoolers. In *Cryocoolers* (Vol. 23, pp. 165–170). Cryocoolers Published in Cryocoolers 23.
- Manoj, K. S., Anbarasu, S., Ghosh, S., & Sarangi, S. (2022). Thermal performance of a single stage double inlet pulse tube refrigerator: Experimental investigation and CFD simulation. *Experimental Heat Transfer*, 35(3), 325–340. <https://doi.org/10.1080/08916152.2021.1873875>
- Marquardt, E., Le, J., & Radebaugh, R. (2002). Cryogenic material properties database. *Cryocoolers*, 11, 681–687. <https://doi.org/10.1007/b115268>
- Matsubara, Y., & Gao, J. (1994). Novel configuration of three-stage pulse tube refrigerator for temperatures below 4 K. *Cryogenics*, 34(4), 259–262. [https://doi.org/10.1016/0011-2275\(94\)90104-X](https://doi.org/10.1016/0011-2275(94)90104-X)
- Mc Carty, R. D. (1973). Thermodynamic properties of helium 4 from 2 to 1500 K at pressures to 108 Pa. *Journal of Physical and Chemical Reference Data*, 2(4), 923–1042. <https://doi.org/10.1063/1.3253133>
- Mikulin, E., Tarasov, A., & Shkrebyonock, M. (1984). Low-temperature expansion pulse tubes. In *Advances in Cryogenic Engineering* (Vol. 29, pp. 629–637). Springer.
- Moudghalya, S., Nerale, M. M., Panda, D., Rajendra Prasad, K. S., Behera, U., & Reddy, B. N. S. (2024). Numerical investigation on non-linear streaming effects in a two-stage coaxial pulse tube cryocooler. *Physics of Fluids*, 36(1), 016124. <https://doi.org/10.1063/5.0178688>
- Mulcahey, T., Conrad, T., & Ghiaasiaan, S. (2012). CFD modeling of tilt induced cooling losses in inertance tube pulse tube cryocoolers. *Cryocoolers*, 17, 143–150.
- Nyborg, W. L. M. (1965). Acoustic streaming. In *Physical acoustics* (Vol. 2, pp. 265–331). Elsevier.

- Panda, D., Satapathy, A. K., & Sarangi, S. K. (2023). Effect of thermal dispersion and turbulent conduction on the heat transfer behavior of coaxial pulse tube cryocooler. *Numerical Heat Transfer, Part A: Applications*, 83(12), 1303–1330. <https://doi.org/10.1080/10407782.2022.2078579>
- Patankar, S. (2018). *Numerical heat transfer and fluid flow*. Taylor & Francis.
- Radebaugh, R. (2000). Pulse tube cryocoolers for cooling infrared sensors. *Infrared Technology and Applications XXVI*, 4130, 363–379. <https://doi.org/10.1117/12.409878>
- Radebaugh, R. (2009). Cryocoolers: The state of the art and recent developments. *Journal of Physics: Condensed Matter*, 21(16), 164219.
- Rout, S., Gupta, A., Choudhury, B., Sahoo, R., & Sarangi, S. (2013). Influence of porosity on the performance of a pulse tube refrigerator: A CFD study. *Procedia Engineering*, 51, 609–616. <https://doi.org/10.1016/j.proeng.2013.01.086>
- Shaowei, Z., Peiyi, W., & Zhongqi, C. (1990). Double inlet pulse tube refrigerators: An important improvement. *Cryogenics*, 30(6), 514–520. [https://doi.org/10.1016/0011-2275\(90\)90051-D](https://doi.org/10.1016/0011-2275(90)90051-D)
- Shiraishi, M., Murakami, M., Nakano, A., & Iida, T. (2007). Visualization of secondary flow in an inclined double-inlet pulse tube.
- Shiraishi, M., Nakamura, N., Murakami, M., & Nakano, A. (1998). Visualization study of flow behavior in pulse tube refrigerators. *TEION KOGAKU (Journal of Cryogenics and Superconductivity Society of Japan)*, 33(4), 249–257. <https://doi.org/10.2221/jcsj.33.249>
- Swift, G. W. (2017). *Thermoacoustics: A unifying perspective for some engines and refrigerators*. Springer.
- Tishin, A. M., & Spichkin, Y. I. (2016). *The magnetocaloric effect and its applications*. CRC Press.
- Walker, G. (2014). *Cryocoolers: Part 1: Fundamentals*. Springer.
- Wang, S., Zhang, T., Gao, Q., Han, Z., Huang, H., & Yao, J. (2024). Performance simulation of L-shaped heat pipe and air coupled cooling process for ternary lithium battery module. *Engineering Applications of Computational Fluid Mechanics*, 18(1), 2301058. <https://doi.org/10.1080/19942060.2023.2301058>
- Yan, C., Zhang, Y., Qiu, J., Chen, Y., Wang, X., Dai, W., Ma, M., Li, H., & Luo, E. (2020). Numerical and experimental study of partly tapered pulse tube in a pulse tube cryocooler. *International Journal of Refrigeration*, 120, 474–480. <https://doi.org/10.1016/j.ijrefrig.2020.09.013>
- Zhang, L., Wu, X., Deng, Z., & Zhao, C. (2024). Performance improvement and numerical study on cathode channel for air-cooled open-cathode proton exchange membrane fuel cells. *Engineering Applications of Computational Fluid Mechanics*, 18(1), 2351958. <https://doi.org/10.1080/19942060.2024.2351958>
- Zhang, N., Wang, Z., Zhang, B., Yang, H., Bao, R., Xiong, S., Du, X., & Min, R. (2024). Performance investigation of battery thermal management system based on L-shaped heat pipe coupled cold plate and optimization of controllable liquid cooling. *Engineering Applications of Computational Fluid Mechanics*, 18(1), 2370941. <https://doi.org/10.1080/19942060.2024.2370941>
- Zhao, Y. (2022). CFD simulation of a micro pulse tube cryocooler operating over 100 Hz without reservoirs. In *2022 IEEE 6th Information Technology and Mechatronics Engineering Conference (ITOEC)* (Vol. 6, pp. 858–862). IEEE.
- Zhao, Y., & Dang, H. (2016). CFD simulation of a miniature coaxial stirling-type pulse tube cryocooler operating at 128 Hz. *Cryogenics*, 73, 53–59. <https://doi.org/10.1016/j.cryogenics.2015.11.007>